Simplified Control Structure of Fuzzy Logic and Kalman Filter for Induction Motor Drive

Dung Quang NGUYEN[1], *Quang Thanh NGUYEN*[1], *Trung Van NGUYEN*[2], *Tai Huu LE*[2], *Hau Huu VO*[3,*], *Pavel BRANDSTETTER*[4]

[1]Faculty of Electrical and Electronics Engineering, Ton Duc Thang University, Ho Chi Minh City, Vietnam
[2]Department for Facility Management, Ton Duc Thang University, Ho Chi Minh City, Vietnam
[3]Modeling Evolutionary Algorithms Simulation and Artificial Intelligence, Faculty of Electrical and Electronics Engineering, Ton Duc Thang University, Ho Chi Minh City, Vietnam
[4]Faculty of Electrical Engineering and Computer Science, VSB–Technical University of Ostrava, Czech

*Corresponding Author: Hau Huu VO (Email: vohuuhau@tdtu.edu.vn)
(Received: 6-Jun-2021; accepted: 29-Jul-2021; published: 30-Sep-2021)
DOI: http://dx.doi.org/10.55579/jaec.202153.334

Abstract. *The paper deals with utilization of Kalman filter and fuzzy logic control in induction motor drive with direct torque control (DTC). In order to lower ripple of stator current vector in DTC drive, pulse width modulation technique with high switching frequency is applied. However, performance of the DTC also depends on the accuracy of both stator resistance and stator current vector. In the paper, the stator resistance and stator current components are assumed to be distorted by Gaussian noises. In order to reduce the effect of noises especially at low speed and very low speed regions, a simple Kalman filter is applied for filtering current components, and fuzzy logic theory is used to increase flexibility of proportional-integral (PI) compensator in the speed controller of the drive structure. Simulations are implemented in conditions of high-level noises of stator current and stator resistance, and a wide range of load torque. An ITAE-based criterion is utilized to evaluate performance of drive structures. Results confirmed the expected dynamic properties of the proposed drive structure.*

Keywords

Induction motor (IM) drive, direct torque control (DTC), Kalman filter (KF), fuzzy logic, ITAE performance index.

1. Introduction

Conventional direct torque control (DTC) technique proposed in the 1980s [1]-[2] were implemented in high-performance applications of induction motor (IM) drives. This technique can be co-ranked with vector control (VC) technique introduced by Hasse and Blaschke [3]-[4], although the control structures with DTC do not contain many complicated frame transformations, current regulators as those with VC [5]-[6]. Robustness of direct torque controlled drive systems is also guaranteed [7]. Several DTC modifications are utilized to reduce ripples of the stator flux, the stator current, and the motor torque. In 12-sector method, locus of stator flux phasor is divided into twelve sectors, and six auxiliary vectors are additively defined [8]. For direct calculation method [9], voltage vector is a weighted sum vector of deviations of motor torque and stator flux. The above methods produce variable switching frequency of voltage source inverter (VSI). Insertion of Pulse-Width Modulation (PWM) into the DTC control structure makes switching frequency constant. Sinusoidal PWM (SPWM) and Space Vector PWM (SVPWM) can be deployed for modulation. Excitation, limitation of stator current, switching losses reduction, total harmonic distortion minimization for both two-level and three-level VSIs are also guaranteed with PWM-DTC [10, 11]. Therefore, it is implemented in both sensor and sensorless IM drives with DTC [10]-[12].

In practical IM drives, any errors in stator resistance and stator current that are inputs of signal calculation block in DTC schemes degrade the IM drive performance especially at low speed and very low speed areas [13]. Sources of the noises are changes of operating conditions, errors in offline/online identification algorithms, offsets, gain errors and gain unbalances in the transduced variables [14]-[16]. In order to reduce stator currents noises, one of most appropriate solutions is Kalman filter (KF) that provides the optimal Bayesian estimates for linear systems which independent Gaussian process and measurement noises are inserted into their dynamics [17]-[18]. For nonlinear systems, Taylor series expansions are applied in extended Kalman filter (EKF) to linearize nonlinear models about working points [19, 20]. In case of highly nonlinear systems, in order to parameterize mean and covariance without linearization steps, a set of points is sampled discretely for Unscented Kalman filter (UKF) [21]. Kitanidis Kalman filter (KKF) and its extended versions (EKKF) are developed and applied for unknown or highly non-Gaussian inputs for both linear and nonlinear systems [22]-[26]. In the paper, there are three assumptions as follows: unknown IM state-space model, high switching frequency of SVPWM technique, Gaussian noises of stator currents and stator resistance. In field of IM drive, various techniques have been combined with KFs to improve performance of estimation. Differential evolution (DE) is utilized to offline optimize the covariance matrices of a KF-based algorithm which estimates the stator-flux linkage components [27]. Kalman filter is employed for the filtration of stator currents and obtaining their derivatives in sensorless IM drive [28]. The motor speed and flux are estimated by a multiple-model EKF with Markov chain [29]. Covariance matrices in EKF have been optimized by using a particle swarm optimization algorithm [30]. An adaptive algorithm is inserted to update system noise covariance matrix in EKF [31]. The system noise covariance matrix is tuned by genetic algorithm [32]. In the paper, improvement of KFs performance is not focused, instead a combination of Kalman filtering and fuzzy logic control is utilized.

Fuzzy logic control (FLC) is chosen because it is able to incorporate experience, intuition and heuristics into the system instead of relying on system dynamics models [33], or simulate behavior of controller [34]. In order to reduce computation time, FLC employs reduced number of fuzzy inference rules in IM drive with DTC [35]. Dynamic FLC is combined with predictive DTC (P-DTC) to reduce the parameter dependency of P-DTC [36]. An adaptive weight genetic algorithm is utilized to find optimum membership functions and control rules in gear shifting fuzzy control of a vehicle equipped with an automated manual transmission [37]. In permanent magnet synchronous motor (PMSM) drive, an adaptive fuzzy logic-based duty cycle vector modulator and an extended Kalman estimator is combined to avoid extra usage of multiple mechanical sensors, reject external perturbations, reduce stator current harmonics and guarantee accurate prediction model in model predictive DTC [38]. In order to reduce rigidity of conventional direct power control and lower power ripples in an active power filter, fuzzy logic-based controller is utilized to replace hysteresis controllers and switching table [39]. FLC is employed in a maximum power point tracking algorithm to get entire energy from PV modules for PMSM drive system [40]. FLC is incorporated into model predictive DTC to get optimal switching states that minimize electromagnetic torque and stator flux errors in PMSM drive [41]. In speed control of BLDC motor, a combination of deep learning and fuzzy logic tunes gain values of PID controller to obtain an effective speed regulator [42]. Estimated position and speed error are optimized with ANFIS and fuzzy-PID methods in sensorless speed control of switched reluctance motor [43]. In IM drive with VC, self-tuning technique is utilized to update the output scaling factor of the main FLC speed controller [44], and a hybrid fuzzy-fuzzy controller that consists of fuzzy slip frequency controller and fuzzy current amplitude controller is developed [45]. A 3-D Mamdani type-2 fuzzy controller gives lower flux and torque ripples than conventional proportional-integral controller in IM drive with DTC [46]. Next, control structure with combination of Kalman filtering and fuzzy logic is described. Simulation results are presented in next section. Finally, conclusions are given.

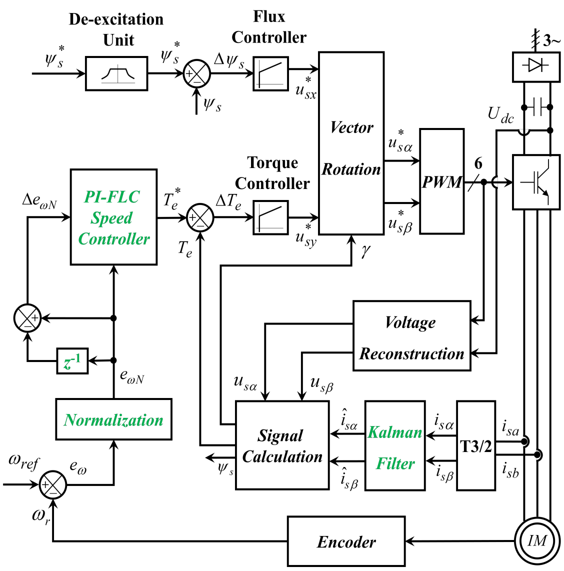

Fig. 1: Proposed drive structure.

2. Proposed control structure of induction motor drive

Figure 1 represents proposed IM drive structure with combination of fuzzy logic and Kalman filter. Stator resistance whose variation affects dominantly to performance of DTC strategy is assumed to be distorted by zero-mean Gaussian noise. Deformations of stator current vector in process and measurement are also produced by the noise. In the combination, Kalman filter is employed to smooth two components of stator current vector, and parameters of proportional-integral (PI) controller are adjusted by fuzzy logic to cope with system uncertainty.

Important quantities of PWM-DTC strategy are obtained according to Eqs. (1)-(5):

$$\psi_{s\alpha} = \int \left(u_{s\alpha} - \hat{i}_{s\alpha} R_s\right) \mathrm{d}t \tag{1}$$

$$\psi_{s\beta} = \int \left(u_{s\beta} - \hat{i}_{s\beta} R_s\right) \mathrm{d}t \tag{2}$$

$$\psi_s = \sqrt{\psi_{s\alpha}^2 + \psi_{s\beta}^2} \tag{3}$$

$$\gamma = \arcsin\left(\psi_{s\beta}/\psi_s\right) \tag{4}$$

$$T_e = (3p/2)\left(\hat{i}_{s\beta}\psi_{s\alpha} - \hat{i}_{s\alpha}\psi_{s\beta}\right) \tag{5}$$

where inputs of Signal Calculation block: $u_{s\alpha}$, $u_{s\beta}$ - stator voltage vector components; $\hat{i}_{s\alpha}, \hat{i}_{s\beta}$ - filtered components of stator current vector; R_s - known value of stator resistance; outputs of the block: ψ_s - magnitude of stator flux vector; γ - orienting angle; T_e - electromagnetic motor torque. Kalman Filter block receives two signal inputs- $i_{s\alpha}$, $i_{s\beta}$ from T3/2 block, and utilizes a compacted Kalman filter algorithm to obtain two signal outputs-$\hat{i}_{s\alpha}, \hat{i}_{s\beta}$ according to Eqs. (6)-(13):

$$\mathbf{x}_k = \mathbf{F}\mathbf{x}_{k-1} + \mathbf{w}_{k-1} \tag{6}$$

$$\mathbf{y}_k = \mathbf{H}\mathbf{x}_k + \mathbf{v}_k \tag{7}$$

$$\tilde{\mathbf{x}}_k = \mathbf{F}\hat{\mathbf{x}}_{k-1} \tag{8}$$

$$\tilde{\mathbf{P}}_k = \mathbf{F}\hat{\mathbf{P}}_{k-1}\mathbf{F}^T + \mathbf{Q} \tag{9}$$

$$\tilde{\mathbf{z}}_k = \mathbf{y}_k - \mathbf{H}\tilde{\mathbf{x}}_k \tag{10}$$

$$\mathbf{K}_k = \tilde{\mathbf{P}}_k\mathbf{H}^T\left(\mathbf{H}\tilde{\mathbf{P}}_k\mathbf{H}^T + \mathbf{R}\right)^{-1} \tag{11}$$

$$\hat{\mathbf{x}}_k = \tilde{\mathbf{x}}_k + \mathbf{K}_k\tilde{\mathbf{z}}_k \tag{12}$$

$$\hat{\mathbf{P}}_k = \left(\mathbf{I} - \mathbf{K}_k\mathbf{H}\right)\tilde{\mathbf{P}}_k \tag{13}$$

where: $\mathbf{x} = [i_{s\alpha} \quad i_{s\beta}]^T$: state vector; $\mathbf{F}$, $\mathbf{H}$: state transition matrix, measurement matrix, they are Identify matrices because of unknown IM model and measuring process; $\mathbf{w}$, $\mathbf{v}$: zero-mean Gaussian process, measurement noise vectors with covariances $\mathbf{Q} = {\sigma_P}^2\mathbf{I}$, $\mathbf{R} = {\sigma_M}^2\mathbf{I}$; symbols $\wedge$, $\sim$ respectively denote estimated, predicted vectors. Next, design of PI-FLC speed controller is carried out.

Speed error e_ω is normalized to $e_{\omega N}$ by dividing the e_ω by maximum value of reference speed ω_{ref}. The $e_{\omega N}$ and its difference $\Delta e_{\omega N}$ have 3 linguistic variables *PO*, *ZE*, *NE* which indicate postive, zero, negative respectively. The *PO*, *ZE*, *NE* have membership functions: Γ-function, Λ-function, *L*-function respectively expressed by Eqs. (14)-(19):

$$\mu_{PO}(e_{\omega N}) = \begin{cases} 1, & e_{\omega N} \geq H_e \\ \dfrac{e_{\omega N}}{H_e}, & 0 \leq e_{\omega N} < H_e \\ 0, & e_{\omega N} < 0 \end{cases} \tag{14}$$

$$\mu_{ZE}(e_{\omega N}) = \begin{cases} 0, & e_{\omega N} \geq H_e \\ \dfrac{H_e - e_{\omega N}}{H_e}, & 0 \leq e_{\omega N} < H_e \\ \dfrac{H_e + e_{\omega N}}{H_e}, & -H_e \leq e_{\omega N} < 0 \\ 0, & e_{\omega N} < 0 \end{cases} \tag{15}$$

$$\mu_{NE}(e_{\omega N}) = \begin{cases} 0, & e_{\omega N} \geqslant 0 \\ -\dfrac{e_{\omega N}}{H_e}, & -H_e \leqslant e_{\omega N} < 0 \\ 1, & e_{\omega N} < -H_e \end{cases} \tag{16}$$

$$\mu_{PO}(\Delta e_{\omega N}) = \begin{cases} 1, & \Delta e_{\omega N} \geqslant H_{\Delta e} \\ \dfrac{\Delta e_{\omega N}}{H_{\Delta e}}, & 0 \leqslant \Delta e_{\omega N} < H_{\Delta e} \\ 0, & \Delta e_{\omega N} < 0 \end{cases} \tag{17}$$

$$\mu_{ZE}(\Delta e_{\omega N}) = \begin{cases} 0, & \Delta e_{\omega N} \geqslant H_{\Delta e} \\ \dfrac{H_{\Delta e} - \Delta e_{\omega N}}{H_{\Delta e}}, & 0 \leqslant \Delta e_{\omega N} < H_{\Delta e} \\ \dfrac{H_{\Delta e} + \Delta e_{\omega N}}{H_{\Delta e}}, & -H_{\Delta e} \leqslant \Delta e_{\omega N} < 0 \\ 0, & \Delta e_{\omega N} < -H_{\Delta e} \end{cases} \tag{18}$$

$$\mu_{NE}(\Delta e_{\omega N}) = \begin{cases} 0, & \Delta e_{\omega N} \geqslant 0 \\ -\dfrac{\Delta e_{\omega N}}{H_{\Delta e}}, & -H_{\Delta e} \leqslant \Delta e_{\omega N} < 0 \\ 1, & \Delta e_{\omega N} < -H_{\Delta e} \end{cases} \tag{19}$$

where limits H_e and $H_{\Delta e}$ are in the domain $(0, 1]$. Fuzzy rule base with 9 rules receives two inputs e_ω, Δe_ω to obtain three linguistic values *L*, *M*, *S* which respectively denote for large, medium, small of controller parameters K_P, $1/T_I$ (see Tab. 1).

Tab. 1: Fuzzy rule base.

Δe_ω	e_ω		
	PO	ZE	NE
PO	L, S	M, S	S, S
ZE	L, M	M, M	S, M
NE	L, L	M, L	S, L

Gaussian membership functions that are defined in Eqs. (20)-(25) are chosen for values L, M, S in because of their smoothness [47]. In order to get crisp values of $K_P, 1/T_I$, centroid method is selected to defuzzify.

$$\mu_L(K_P) = \begin{cases} 1, & K_P \geqslant M_P \\ e^{-\frac{(K_P - M_P)^2}{2\sigma_1^2}}, & m_P < K_P < M_P \\ 0, & K_P \leqslant m_P \end{cases} \tag{20}$$

$$\mu_M(K_P) = \begin{cases} 0, & K_P \geqslant M_P \\ e^{-\frac{(K_P - C_P)^2}{2\sigma_1^2}}, & m_P < K_P < M_P \\ 0, & K_P \leqslant m_P \end{cases} \tag{21}$$

$$\mu_S(K_P) = \begin{cases} 0, & K_P \geqslant M_P \\ e^{-\frac{(K_P - m_P)^2}{2\sigma_1^2}}, & m_P < K_P < M_P \\ 1, & K_P \leqslant m_P \end{cases} \tag{22}$$

$$\mu_L(1/T_I) = \begin{cases} 1, & 1/T_I \geqslant M_I \\ e^{-\frac{(1/T_I - M_I)^2}{2\sigma_2^2}}, & m_I < 1/T_I < M_I \\ 0, & 1/T_I \leqslant m_I \end{cases} \tag{23}$$

$$\mu_M(1/T_I) = \begin{cases} 0, & 1/T_I \geqslant M_I \\ e^{-\frac{(1/T_I - C_I)^2}{2\sigma_2^2}}, & m_I < 1/T_I < M_I \\ 0, & 1/T_I \leqslant m_I \end{cases} \tag{24}$$

$$\mu_S(1/T_I) = \begin{cases} 0, \ 1/T_I \geqslant M_I \\ e^{-\frac{(1/T_I - m_I)^2}{2\sigma_2^2}}, m_I < 1/T_I < M_I \\ 1, \ 1/T_I \leqslant m_I \end{cases} \tag{25}$$

where $0 < m_P < M_P$, $0 < m_I < M_I$. Remaining parameters are chosen so that symmetry of membership functions graphs is ensured, and intersections between membership functions for pairs of variables L & M, S & M have a value of 0.5 as in Eqs. (26)-(29):

$$C_P = (m_P + M_P)/2 \tag{26}$$

$$\sigma_1^2 = (M_P - m_P)^2 \Big/ (32 \ln 2) \tag{27}$$

$$C_I = (m_I + M_I)/2 \tag{28}$$

$$\sigma_2^2 = (M_I - m_I)^2 \Big/ (32 \ln 2) \tag{29}$$

3. Simulation results

In this section, simulations are implemented on Matlab/Simulink environment with IM parameters given in Tab. 2 at reference speeds of 60 rpm and 6 rpm that represent low and very low speed ranges respectively. The VSI has input of 540 Vdc and switching diagrams of 6 IGBTs are based on SVPWM method with frequency of 20 kHz. Reference torque - output of speed controller in drive structures is limited in range ±14 Nm. Graphs of important quantities are recorded with load torque and reference speeds shown in Figs. 2-3.

Tab. 2: IM specifications.

Parameter	Value
Rated power	2.2 kW
Rated speed	1420 rpm
Rated voltage	230 V/400 V
Rated torque	14.8 Nm
Number of pole pairs	2
Moment of inertia	0.0047 kgm^2
Stator resistance	3.179 W
Stator inductance	0.209 H
Mutual inductance	0.192 H
Rotor resistance	2.118 W
Rotor time constant	0.0987 s

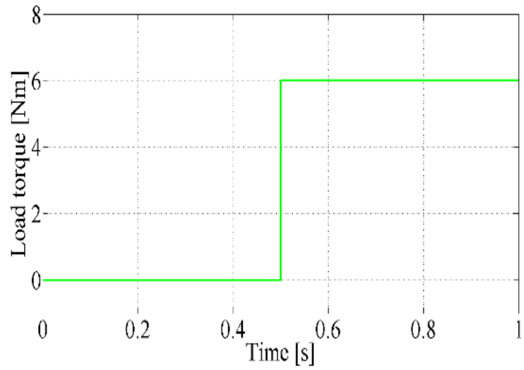

Fig. 2: Load torque with load jump = 6 Nm at time 0.5s.

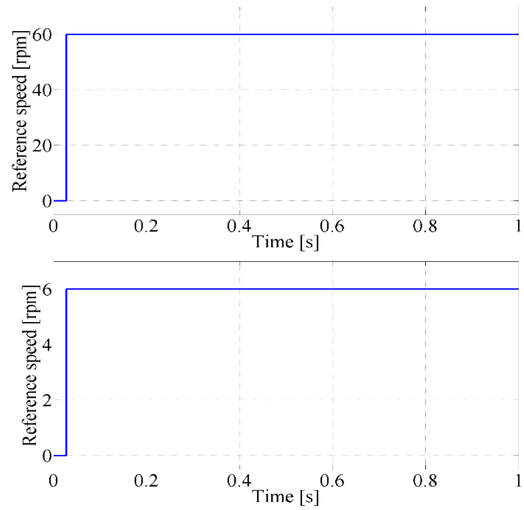

Fig. 3: Reference speeds $\omega_{\mathrm{ref}} = 60$ rpm and 6 rpm.

For simplicity, assume that, ${\sigma_P}^2 = {\sigma_M}^2 = K_\sigma$ and variance of added relative value of stator resistance is K_r. For performance comparison of drive structures, Integral Time Absolute Error (ITAE) performance index (see Eq. (30)) is selected. Ratios of ITAE indices (RITAE) are used to compare between proposed structure and drive structure described in [7]:

$$\mathrm{ITAE} = \int_0^1 t|e_\omega(t)|\mathrm{d}t \tag{30}$$

$$\mathrm{RITAE_{KF}} = \mathrm{ITAE_{KF}}/\mathrm{ITAE_{CO}} \tag{31}$$

$$\mathrm{RITAE_{PR}} = \mathrm{ITAE_{PR}}/\mathrm{ITAE_{CO}} \tag{32}$$

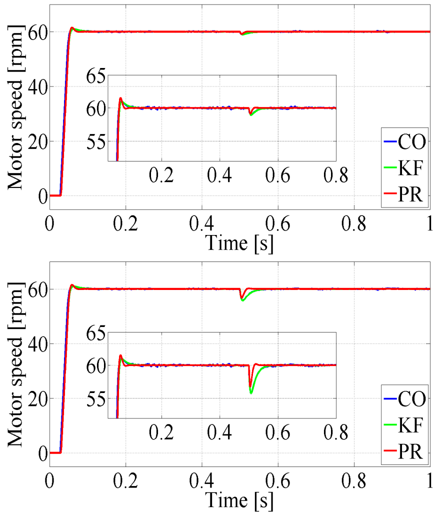

Fig. 4: Speed at $\omega_{\mathrm{ref}} = 60$ rpm, $K_\sigma = 0.5^2, K_r = 0.01^2$, load jump 2 Nm (upper) and 8 Nm.

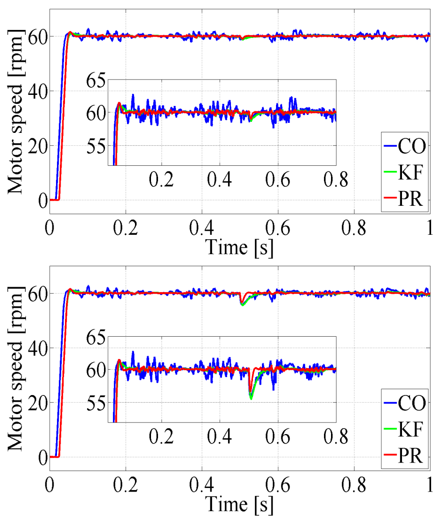

Fig. 5: Speed at $\omega_{\mathrm{ref}} = 60$ rpm, $K_\sigma = 1.5^2, K_r = 0.01^2$, load jump 2 Nm (upper) and 8 Nm.

where subscripts *CO*, *KF*, and *PR* represent conventional drive structure, one with Kalman filtering, and proposed one respectively. Speed controller in *CO* and *KF* structures has K_P = 1.5, T_I = 0.05s. For PR structure, selection of m_P, M_P, m_I, M_I is similar to that in [12]: m_P = 0.1, M_P =2.9, m_I = 27.12, M_I = 320. Limits H_e and $H_{\Delta e}$ are chosen experimentally as follows $H_e = 0.16$, $H_{\Delta e} = 0.0009$. Simulations are obtained with 4 values of load jump, noises of stator resistance and stator current.

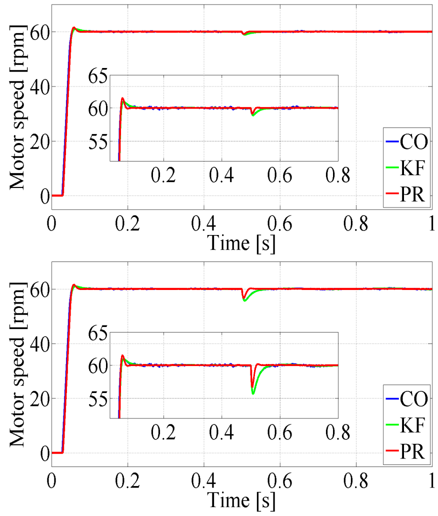

Fig. 6: Speed at $\omega_{\mathrm{ref}} = 60$ rpm, $K_\sigma = 0.5^2, K_r = 0.04^2$, load jump 2 Nm (upper) and 8 Nm.

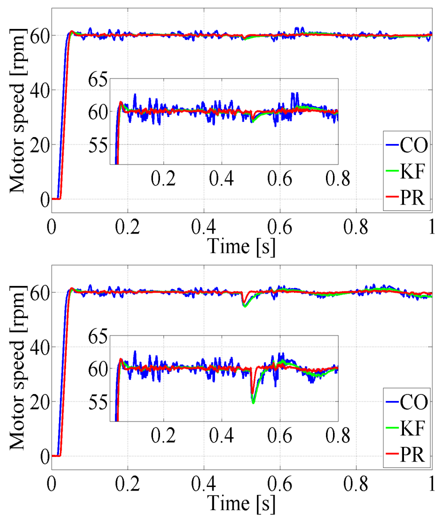

Fig. 7: Speed at $\omega_{\mathrm{ref}} = 60$ rpm, $K_\sigma = 1.5^2, K_r = 0.04^2$, load jump 2 Nm (upper) and 8 Nm.

Figures 4-11 show motor speed responses obtained with minimum or maximum simulated values of K_σ, K_r, and load jump for both speed regions. Overshoot and undershoot of speed responses for three drive structures are listed in Tabs. 3-4. It is easy to see that overshoots for KF structure are lowest ones in most cases, and undershoots for PR structure are smallest ones in all cases.

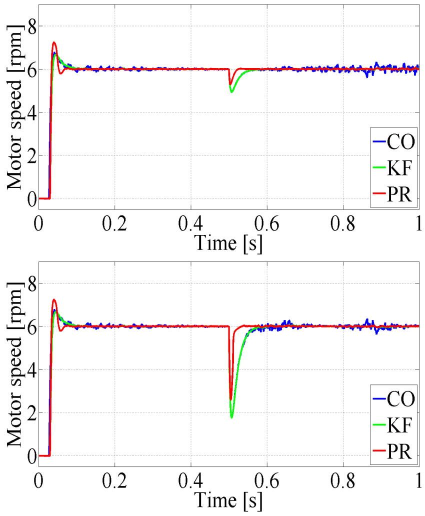

Fig. 8: Speed at $\omega_{\text{ref}} = 6$ rpm, $K_\sigma = 0.5^2, K_r = 0.01^2$, load jump 2 Nm (upper) and 8 Nm.

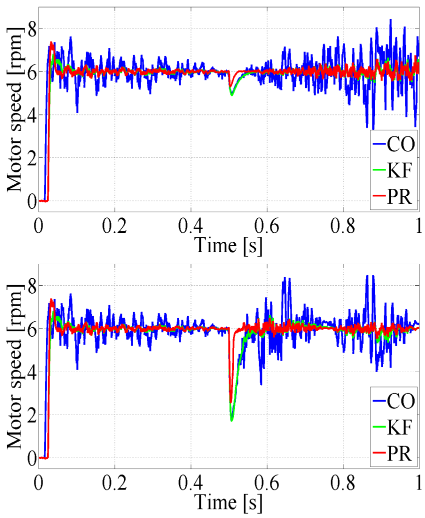

Fig. 9: Speed at $\omega_{\text{ref}} = 6$ rpm, $K_\sigma = 0.5^2, K_r = 0.04^2$, load jump 2 Nm (upper) and 8 Nm.

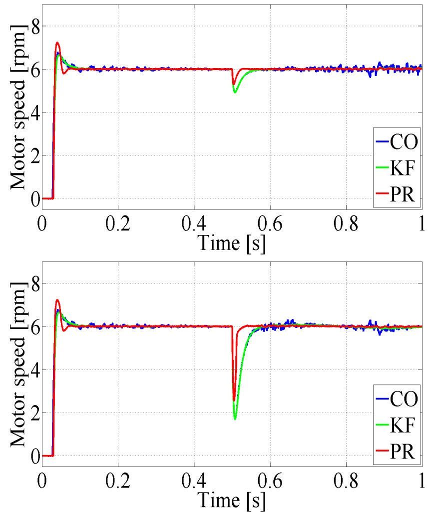

Fig. 10: Speed at $\omega_{\text{ref}} = 6$ rpm, $K_\sigma = 1.5^2, K_r = 0.01^2$, load jump 2 Nm (upper) and 8 Nm.

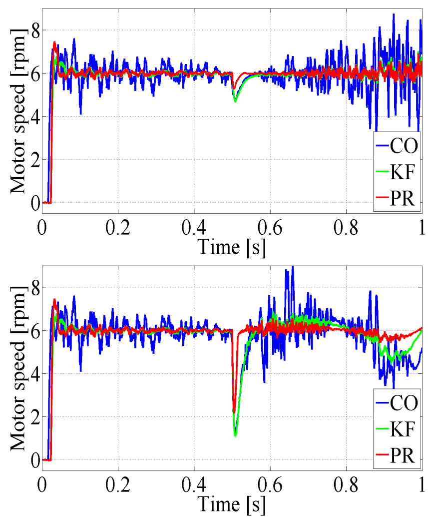

Fig. 11: Speed at $\omega_{\text{ref}} = 6$ rpm, $K_\sigma = 1.5^2, K_r = 0.04^2$, load jump 2 Nm (upper) and 8 Nm.

Settling times t_{ss1}, t_{ss2} are searched in durations 0.0s-0.5s, 0.5s-1.0s, and listed in Tabs. 5-6 respectively. Letter "X" in the tables describes the fact that t_{ss1} or t_{ss2} can not be found. In most cases, t_{ss1} and t_{ss2} are shortest for KF structure and PR structure respectively. For PR structrure, increment in difference $(M_I - m_I)$ tends to reduce speed error [12] or ITAE, shorten settling times, make overshoots higher. RITAEs at low speed and very low speed areas are respectively listed in Tabs. 7-10 and Tabs. 11-14.

All RITAEs are less than one. RITAE at low speed is greater than one at very low speed in same condition of load jump, K_σ and K_r for both KF and PR structures. For low speed, RITAEs for PR structure are approximately 18%-59% lower than those for KF structure, in cases of very low speed, those for PR structure are roughly 20%-67% smaller than those for KF

Tab. 3: Overshoot and undershoot at 60 rpm.

K_σ	K_r	Load jump	Overshoot CO	Overshoot KF	Overshoot PR	Undershoot CO	Undershoot KF	Undershoot PR
0.5^2	0.01^2	2	0.94	0.94	1.51	1.08	1.10	0.85
0.5^2	0.01^2	8				4.24	4.29	3.30
1.5^2	0.01^2	2	2.76	0.95	1.50	2.37	1.39	1.04
1.5^2	0.01^2	8				4.29	4.57	3.38
0.5^2	0.04^2	2	0.93	0.94	1.50	1.12	1.14	0.87
0.5^2	0.04^2	8				4.34	4.37	3.34
1.5^2	0.04^2	2	2.67	0.90	1.47	2.30	1.68	1.20
1.5^2	0.04^2	8				5.16	5.35	3.85

Tab. 4: Overshoot and undershoot at 6 rpm.

K_σ	K_r	Load jump	Overshoot CO	Overshoot KF	Overshoot PR	Undershoot CO	Undershoot KF	Undershoot PR
0.5^2	0.01^2	2	0.80	0.67	1.25	1.06	1.07	0.72
0.5^2	0.01^2	8				4.25	4.25	3.42
1.5^2	0.01^2	2	1.62	0.80	1.38	2.79	1.13	0.71
1.5^2	0.01^2	8				4.28	4.29	3.45
0.5^2	0.04^2	2	0.80	0.66	1.23	1.08	1.09	0.72
0.5^2	0.04^2	8				4.30	4.31	3.46
1.5^2	0.04^2	2	1.60	0.80	1.47	2.93	1.35	0.73
1.5^2	0.04^2	8				4.78	4.90	3.84

Tab. 5: Settling times at 60 pm.

K_σ	K_r	Load jump	$t_{ss1}[\times 10^{-3}s]$ CO	t_{ss1} KF	t_{ss1} PR	$t_{ss2}[\times 10^{-3}s]$ CO	t_{ss2} KF	t_{ss2} PR
0.5^2	0.01^2	2	35	37	46	0	0	0
0.5^2	0.01^2	8				32	32	12
1.5^2	0.01^2	2	458	32	41	496	9	0
1.5^2	0.01^2	8				493	33	13
0.5^2	0.04^2	2	35	37	46	0	0	0
0.5^2	0.04^2	8				33	33	13
1.5^2	0.04^2	2	484	31	40	496	16	8
1.5^2	0.04^2	8				X	X	14

structure. The main reason for this is that PR structure gives significantly smaller undershoot than KF structure. Lowest values occur in condition of $K_r = 0.01^2$, load jump = 2 Nm, and highest ones happen in case of $K_r = 0.04^2$, load jump = 8 Nm. Figures 12-14 respectively show stator current components, stator flux components, and motor torque in condition of ω_{ref} = 60 rpm, $K_\sigma = 1.5^2$, $K_r = 0.4^2$, load jump = 8 Nm.

Tab. 6: Settling times at 6 rpm.

K_σ	K_r	Load jump	$t_{ss1}[\times 10^{-3}s]$ CO	t_{ss1} KF	t_{ss1} PR	$t_{ss2}[\times 10^{-3}s]$ CO	t_{ss2} KF	t_{ss2} PR
0.5^2	0.01^2	2	170	63	48	496	47	18
0.5^2	0.01^2	8				460	68	22
1.5^2	0.01^2	2	484	428	428	X	X	X
1.5^2	0.01^2	8				500	471	476
0.5^2	0.04^2	2	170	63	47	500	48	18
0.5^2	0.04^2	8				462	419	22
1.5^2	0.04^2	2	484	480	429	X	X	X
1.5^2	0.04^2	8				500	497	477

Tab. 7: RITAEs at Ω_{ref}= 60 rpm, load jump = 2 Nm.

K_r	K_σ = 0.5^2 KF	0.5^2 PR	0.75^2 KF	0.75^2 PR	1.0^2 KF	1.0^2 PR	1.5^2 KF	1.5^2 PR
0.01^2	0.73	0.56	0.55	0.42	0.43	0.34	0.33	0.27
0.02^2	0.76	0.55	0.59	0.42	0.49	0.34	0.40	0.27
0.03^2	0.78	0.54	0.64	0.41	0.55	0.34	0.48	0.27
0.04^2	0.81	0.53	0.68	0.41	0.61	0.34	0.54	0.27

Tab. 8: RITAEs at Ω_{ref}= 60 rpm, load jump = 4 Nm.

K_r	K_σ = 0.5^2 KF	0.5^2 PR	0.75^2 KF	0.75^2 PR	1.0^2 KF	1.0^2 PR	1.5^2 KF	1.5^2 PR
0.01^2	0.78	0.52	0.61	0.42	0.49	0.35	0.37	0.29
0.02^2	0.80	0.51	0.66	0.42	0.55	0.35	0.46	0.29
0.03^2	0.83	0.51	0.71	0.42	0.62	0.35	0.55	0.30
0.04^2	0.86	0.51	0.76	0.42	0.69	0.36	0.64	0.30

The KF gives lower ripples of stator current, stator flux, and motor torque than the CO [7]. Responses for the PR are almost identifical to those for the KF (see Figs. 12-14), because the PR inherits advantages of Kalman filtering from the KF. Moreover, performance of the PR is further enhanced by wide operation condition coverage of fuzzy logic, especially at the time after load activation (see the overshoot of torque responses duration 0.5s-1.0s in Figs. 7 & 14). The peak torque at the time 0.5086s shows the flexibility of fuzzy logic. This brings lower undershoot and smaller t_{ss2} of speed responses in most simulated cases.

Tab. 9: RITAEs at Ω_{ref}= 60 rpm, load jump = 6 Nm.

K_r	K_σ							
	0.5^2		0.75^2		1.0^2		1.5^2	
	KF	PR	KF	PR	KF	PR	KF	PR
0.01^2	0.81	0.48	0.63	0.39	0.52	0.33	0.40	0.27
0.02^2	0.84	0.47	0.69	0.39	0.59	0.33	0.49	0.27
0.03^2	0.86	0.47	0.74	0.38	0.66	0.33	0.59	0.28
0.04^2	0.88	0.46	0.78	0.38	0.72	0.33	0.66	0.29

Tab. 10: RITAEs at Ω_{ref}= 60 rpm, load jump = 8 Nm.

K_r	K_σ							
	0.5^2		0.75^2		1.0^2		1.5^2	
	KF	PR	KF	PR	KF	PR	KF	PR
0.01^2	0.82	0.45	0.67	0.38	0.56	0.33	0.44	0.28
0.02^2	0.85	0.45	0.73	0.38	0.65	0.34	0.57	0.29
0.03^2	0.88	0.45	0.79	0.39	0.73	0.35	0.69	0.31
0.04^2	0.90	0.45	0.83	0.39	0.80	0.36	0.76	0.31

Tab. 11: RITAEs at Ω_{ref}= 6 rpm, load jump = 2 Nm.

K_r	K_σ							
	0.5^2		0.75^2		1.0^2		1.5^2	
	KF	PR	KF	PR	KF	PR	KF	PR
0.01^2	0.50	0.26	0.37	0.23	0.29	0.21	0.25	0.20
0.02^2	0.51	0.25	0.37	0.23	0.30	0.21	0.25	0.20
0.03^2	0.51	0.25	0.38	0.23	0.31	0.20	0.26	0.19
0.04^2	0.52	0.25	0.39	0.23	0.31	0.20	0.27	0.19

Tab. 12: RITAEs at Ω_{ref}= 6 rpm, load jump = 4 Nm.

K_r	K_σ							
	0.5^2		0.75^2		1.0^2		1.5^2	
	KF	PR	KF	PR	KF	PR	KF	PR
0.01^2	0.67	0.27	0.51	0.24	0.40	0.22	0.30	0.20
0.02^2	0.68	0.27	0.53	0.24	0.42	0.22	0.32	0.20
0.03^2	0.70	0.27	0.55	0.24	0.45	0.22	0.34	0.19
0.04^2	0.72	0.26	0.58	0.24	0.48	0.22	0.37	0.19

Tab. 13: RITAEs at Ω_{ref}= 6 rpm, load jump = 6 Nm.

K_r	K_σ							
	0.5^2		0.75^2		1.0^2		1.5^2	
	KF	PR	KF	PR	KF	PR	KF	PR
0.01^2	0.74	0.28	0.57	0.25	0.45	0.23	0.36	0.21
0.02^2	0.76	0.28	0.60	0.25	0.49	0.23	0.40	0.22
0.03^2	0.78	0.28	0.63	0.25	0.53	0.24	0.44	0.22
0.04^2	0.80	0.28	0.66	0.25	0.58	0.24	0.49	0.23

Tab. 14: RITAEs at Ω_{ref}= 6 rpm, load jump = 8 Nm.

K_r	K_σ							
	0.5^2		0.75^2		1.0^2		1.5^2	
	KF	PR	KF	PR	KF	PR	KF	PR
0.01^2	0.78	0.28	0.61	0.25	0.50	0.22	0.38	0.20
0.02^2	0.81	0.28	0.67	0.25	0.57	0.23	0.47	0.21
0.03^2	0.84	0.28	0.72	0.26	0.65	0.24	0.58	0.22
0.04^2	0.87	0.29	0.77	0.26	0.71	0.25	0.56	0.20

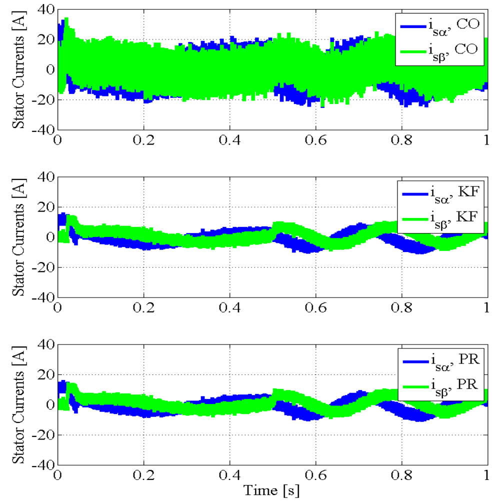

Fig. 12: Stator current components at ω_{ref} = 60 rpm, $K_\sigma = 1.5^2, K_r = 0.04^2$, load jump = 8 Nm.

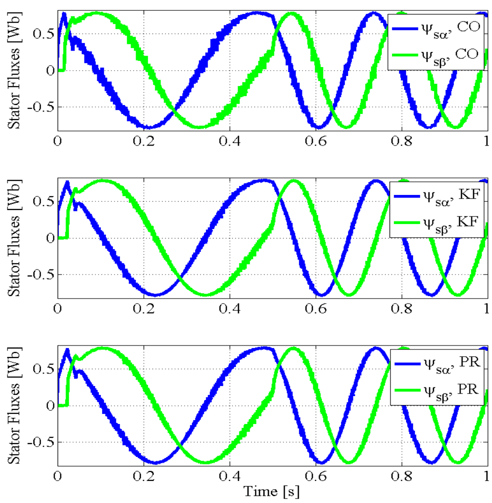

Fig. 13: Stator flux components at ω_{ref} = 60 rpm, $K_\sigma = 1.5^2, K_r = 0.04^2$, load jump = 8 Nm.

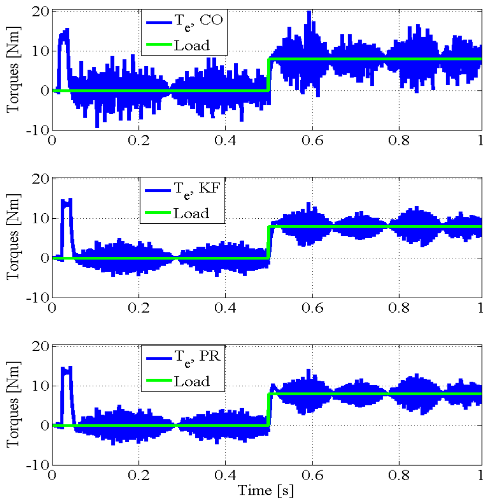

Fig. 14: Torques at $\omega_{\text{ref}} = 60$ rpm, $K_\sigma = 1.5^2, K_r = 0.04^2$, load jump = 8 Nm.

4. Conclusions

Simplified structure using FLC and KF was presented in the paper. Simulations were implemented at two low speed and very low-speed regions in different conditions of load jumps, noise covariances of stator resistance and stator currents. The proposed control structure with simplified fuzzy logic controller and Kalman filtering brought lower values of ITAE performance index than both the conventional and the KF ones at both speed regions, wide ranges of load jump and noises. This structure gave shorter settling times and smaller undershoot in duration of load activation than two other ones. Type-2 fuzzy controllers or robust controllers can be utilized to get better performance. The proposed method can be applied in sensorless control, fault-tolerant control of IM drive.

References

[1] Takahashi, I., & Noguchi, T. (1986). A new quick-response and high-efficiency control strategy of an induction motor. *IEEE Transactions on Industry applications, 5*, 820-827.

[2] Depenbrock, M. (1987). Direct self-control (DSC) of inverter fed induktion machine. *In 1987 IEEE Power Electronics Specialists Conference (pp. 632-641)*. IEEE.

[3] Hasse, K. (1969). Zur Dynamik Drehzahlgeregelter Antriebe mit stromrichtergespeisten Asynchron-kurschlusslaüfer Maschinen. Ph.D. dissertation, Technical University of Darmstadt, Darmstadt, Germany.

[4] Blaschke, F. (1972). The principle of field orientation as applied to the new transvektor closed-loop control system for rotating field machines. *Siemens review, 34*(1).

[5] Casadei, D., Serra, G., Tani, A., & Zarri, L. (2013, March). Direct torque control for induction machines: a technology status review. *In 2013 IEEE Workshop on Electrical Machines Design, Control and Diagnosis (WEMDCD) (pp. 117-129)*. IEEE.

[6] Hakami, S. S., Alsofyani, I. M., & Lee, K. B. (2019). Torque ripple reduction and flux-droop minimization of DTC with improved interleaving CSFTC of IM Fed by three-level NPC inverter. *IEEE Access, 7*, 184266-184275.

[7] Vo, H. H., Nguyen, D. Q., Nguyen, Q. T., Dong, C. S. T., Tran, T. C., & Brandstetter, P. (2021). Pulse-width modulation direct torque control induction motor drive with Kalman filter. *Telkomnika, 19*(1), 277-284.

[8] Kumar, B. S., Gupta, R. A., & Kumar, R. (2006, October). 12-sector methodology of torque ripple reduction in a direct torque controlled induction motor drive. *In 2006 SICE-ICASE International Joint Conference (pp. 3587-3592)*. IEEE.

[9] Brandstetter, P., Chlebis, P., & Palacky, P. (2010). Direct torque control of induction motor with direct calculation of voltage vector. *Advances in Electrical and Computer Engineering, 10*(4), 17-22.

[10] Aberkane, H., Sakri, D., & Rahem, D. (2018, March). Comparative study of different variants of direct torque control applied

to induction motor. *In 2018 9th International Renewable Energy Congress (IREC) (pp. 1-6)*. IEEE.

[11] Vaezi, S. A., Iman-Eini, H., & Razi, R. (2019, February). A new space vector modulation technique for reducing switching losses in induction motor DTC-SVM scheme. *In 2019 10th International Power Electronics, Drive Systems and Technologies Conference (PEDSTC) (pp. 184-188)*. IEEE.

[12] Vo, H. H., Kuchar, M., & Brandstetter, P. (2020). Application of fuzzy logic in sensorless induction motor drive with PWM-DTC. *Electrical Engineering, 102*, 129–140.

[13] Buja, G., & Menis, R. (2008). Steady-state performance degradation of a DTC IM drive under parameter and transduction errors. *IEEE Transactions on Industrial Electronics, 55*(4), 1749-1760.

[14] He, L., Cheng, S., Du, Y., Harley, R. G., & Habetler, T. G. (2014). Stator temperature estimation of direct-torque-controlled induction machines via active flux or torque injection. *IEEE Transactions on Power Electronics, 30*(2), 888-899.

[15] Holakooie, M. H., Ojaghi, M., & Taheri, A. (2018). Direct torque control of six-phase induction motor with a novel MRAS-based stator resistance estimator. *IEEE Transactions on Industrial Electronics, 65*(10), 7685-7696.

[16] Luo, C., Wang, B., Yu, Y., Chen, C., Huo, Z., & Xu, D. (2019). Decoupled stator resistance estimation for speed-sensorless induction motor drives considering speed and load torque variations. *IEEE Journal of Emerging and Selected Topics in Power Electronics, 8*(2), 1193-1207.

[17] Kalman, R. E. (1960). A new approach to linear filtering and prediction problems. *Transactions of the ASME–Journal of Basic Engineering, 82*(1), 35-45.

[18] Kalman, R. E., & Bucy, R. S. (1961). New results in linear filtering and prediction theory. *Transactions of the ASME–Journal of Basic Engineering, 83*(1), 95-108.

[19] McElhoe, B. A. (1966). An assessment of the navigation and course corrections for a manned flyby of mars or venus. *IEEE Transactions on Aerospace and Electronic Systems, 4*, 613-623.

[20] Le Anh, T. (2017). Application of extended Kalman filtering for estimating immeasurable vehicle state variables. *Journal of Advanced Engineering and Computation, 1*(1), 18-28.

[21] Julier, S. J., & Uhlmann, J. K. (1997). New extension of the Kalman filter to nonlinear systems. *Proceedings of the SPIE 3068, Signal Processing, Sensor Fusion, and Target Recognition VI, Orlando, FL, USA*, 182-193.

[22] Kitanidis, P. K. (1987). Unbiased minimum-variance linear state estimation. *Automatica, 23*(6), 775-778.

[23] Darouach, M., & Zasadzinski, M. (1997). Unbiased minimum variance estimation for systems with unknown exogenous inputs. *Automatica, 33*(4), 717-719.

[24] Darouach, M., Zasadzinski, M., & Boutayeb, M. (2003). Extension of minimum variance estimation for systems with unknown inputs. *Automatica, 39*(5), 867-876.

[25] Ganesh, C., Ballal, P., Bhushan, M., & Patwardhan, S. C. (2015). Leak identification using extended Kitanidis-Kalman filter. *In Computer Aided Chemical Engineering, 37*, 1817-1822.

[26] Varshney, D., Bhushan, M., & Patwardhan, S. C. (2019). State and parameter estimation using extended Kitanidis Kalman filter. *Journal of Process Control, 76*, 98-111.

[27] Salvatore, N., Caponio, A., Neri, F., Stasi, S., & Cascella, G. L. (2009). Optimization of delayed-state Kalman-filter-based algorithm via differential evolution for sensorless control of induction motors. *IEEE Transactions on Industrial Electronics, 57*(1), 385-394.

[28] Brandstetter, P., Dobrovsky, M., Petrtyl, O., Dong, C. S. T., & Vo, H. H. (2016). Sensorless control of induction motor drive using BEMF-MRAS with Kalman filter. *In 2016 ELEKTRO (pp. 121-126).* IEEE.

[29] Yin, Z., Li, G., Zhang, Y., Liu, J., Sun, X., & Zhong, Y. (2016). A speed and flux observer of induction motor based on extended Kalman filter and Markov chain. *IEEE Transactions on Power Electronics, 32*(9), 7096-7117.

[30] Song, B., Xu, J., & Xu, L. (2018). PSO-based extended kalman filtering for speed estimation of an induction motor. *In 2018 37th Chinese Control Conference (CCC) (pp. 3803-3807).* IEEE.

[31] Zerdali, E. (2018). Adaptive extended Kalman filter for speed-sensorless control of induction motors. *IEEE Transactions on Energy Conversion, 34*(2), 789-800.

[32] Alonge, F., D'Ippolito, F., Fagiolini, A., Garraffa, G., Raimondi, F. M., & Sferlazza, A. (2019). Tuning of Extended Kalman Filters for Sensorless Motion Control with Induction Motor. *In 2019 AEIT International Conference of Electrical and Electronic Technologies for Automotive (AEIT AUTOMOTIVE) (pp. 1-6).* IEEE.

[33] Cirstea, M., Dinu, A., McCormick, M., & Khor, J. G. (2002). Neural and fuzzy logic control of drives and power systems. Elsevier.

[34] Nguyen, T. B. T. (2017). Adaptive MIMO Controller Design for Chaos Synchronization in Coupled Josephson Junctions via Fuzzy Neural Networks. *Journal of Advanced Engineering and Computation, 1*(1), 80-86.

[35] Gdaim, S., Mtibaa, A., & Mimouni, M. F. (2014). Design and experimental implementation of DTC of an induction machine based on fuzzy logic control on FPGA. *IEEE Transactions on Fuzzy Systems, 23*(3), 644-655.

[36] Berzoy, A., Rengifo, J., & Mohammed, O. (2017). Fuzzy predictive DTC of induction machines with reduced torque ripple and high-performance operation. *IEEE Transactions on Power Electronics, 33*(3), 2580-2587.

[37] Eckert, J. J., Santiciolli, F. M., Yamashita, R. Y., Corrêa, F. C., Silva, L. C., & Dedini, F. G. (2019). Fuzzy gear shifting control optimisation to improve vehicle performance, fuel consumption and engine emissions. *IET Control Theory & Applications, 13*(16), 2658-2669.

[38] Benhamida, I., Ameur, A., Kouzi, K., & Gaoui, B. (2019). Torque ripple minimization in predictive torque control method of PMSM drive using adaptive fuzzy logic modulator and EKF estimator. *Journal of Control, Automation and Electrical Systems, 30*(6), 1007-1018.

[39] Kadem, M., Semmah, A., Wira, P., & Dahmani, S. (2020). Fuzzy logic-based instantaneous power ripple minimization for direct power control applied in a shunt active power filter. *Electrical Engineering, 102*(3), 1327-1338.

[40] Anwer, A. M. O., Omar, F. A., & Kulaksiz, A. A. (2020). Design of a Fuzzy Logic-based MPPT Controller for a PV System Employing Sensorless Control of MRAS-based PMSM. *International Journal of Control, Automation and Systems, 18*, 2788-2797.

[41] Justo, J. J., Mwasilu, F., Kim, E. K., Kim, J., Choi, H. H., & Jung, J. W. (2017). Fuzzy model predictive direct torque control of IPMSMs for electric vehicle applications. *IEEE/ASME Transactions on Mechatronics, 22*(4), 1542-1553.

[42] Gobinath, S., & Madheswaran, M. (2019). Deep perceptron neural network with fuzzy PID controller for speed control and stability analysis of BLDC motor. *Soft Computing, 24*, 10161–10180.

[43] Murugan, L. S., & Maruthupandi, P. (2020). Sensorless speed control of 6/4-pole switched reluctance motor with ANFIS and fuzzy-PID-based hybrid observer. *Electrical Engineering, 102*(2), 831-844.

[44] Farah, N., Talib, M. H. N., Shah, N. S. M., Abdullah, Q., Ibrahim, Z., Lazi, J. B. M., & Jidin, A. (2019). A novel self-tuning fuzzy logic controller based induction motor drive system: an experimental approach. I*EEE Access, 7*, 68172-68184.

[45] Magzoub, M., Saad, N., Ibrahim, R., & Irfan, M. (2019). An experimental demonstration of hybrid fuzzy-fuzzy space-vector control on AC variable speed drives. *Neural Computing and Applications, 31*(2), 777-792.

[46] Singh, S. P., & Panda, A. K. (2020). An interval type-2 fuzzy-based DTC of IMD using hybrid duty ratio control. *IEEE Transactions on Power Electronics, 35*(8), 8443-8451.

[47] Nguyen, H. T., Prasad, N. R., Walker, C. L., & Walker, E. A. (2002). A first course in fuzzy and neural control. CRC press.

About Authors

Dung Quang NGUYEN received his MSc degree from Tomsk Polytechnic University, Tomsk City, Russia in 2012. He is now a PhD Student at Faculty of Electrical and Electronics Engineering (FEEE), Ton Duc Thang University (TDTU), Vietnam. His research interests include applications of Kalman filter in control systems; identification and synthesis in fractional, distributed parameter systems; non-linear system; PLC and SCADA system, industrial communication networks, image processing.

Quang Thanh NGUYEN hold his MSc degree from TDTU, Vietnam in 2019. He is preparing to become a PhD Student at FEEE, TDTU, Vietnam. His research interests include applications of intelligent control in electrical drives, microcontrollers, robotics, SCADA.

Trung Van NGUYEN obtain his MSc degree from Ho Chi Minh City University of Transport, Vietnam in 2020. He is preparing to become a PhD Student at FEEE, TDTU, Vietnam. His research interests include applications of intelligent control in microcontrollers and electrical drives.

Tai Huu LE received his MSc degree from University of Transport and Communications, Vietnam in 2015. He is preparing to become a PhD Student at FEEE, TDTU, Vietnam. His research interests include industrial automation and electrical drives.

Hau Huu VO hold a PhD degree from Technical University of Ostrava (VSB-TUO), Czech Republic in 2017. He has been working as a Lecturer at FEEE, TDTU, Vietnam. He has published 10 conference papers and 8 journal papers. His current research interests are intelligent electrical drives.

Pavel BRANDSTETTER completed his PhD degree at Brno University in 1987. He is now full professor at VSB-TUO, Czech Republic. He has published more than 65 conference papers and 30 journal papers. His research interests are intelligent methods in electrical drives and power electronics.

